# Remote Localization of an Underground Acoustic Source by a Passive Sonar System

Soon Suck Jarng
Dept. of Control & Instrumentation Eng., Chosun Uni., South Korea
(Tel:+82-62-230-7107, ssjarng@mail.chosun.ac.kr)

Abstract

The aim of the work described in this paper is to develop a complex underground acoustic system which detects and localizes the origin of an underground hammering sound using an array of hydrophones located about 100m underground. Three different methods for the sound localization will be presented, a time-delay method, a power-attenuation method and a hybrid method. In the time-delay method, the cross correlation of the signals received from the array of sensors is used to calculate the time delays between those signals. In the power-attenuation method, the powers of the received signals provide a measure of the distances of the source from the sensors. A new hybrid method has been developed for estimating the origin of the underground acoustic source by coupling both methods. The Nelder-Meade simplex search algorithm is then used to numerically estimate the position of the source in those methods. For each method the sound localization is carried out in three dimensions underground. The distance between the true and estimated origins of the source is in some cases less than 6m for a search area of radius 250m.

## 1. INTRODUCTION

The ability to detect and determine the position of an underground sound source is desirable both for civilian and military purposes, for example, for rescue following collapse of mining tunnels, or for the detection of covert underground operations.[1,2,3] Compared to the similar problem in air or in water there are a number of features which cause additional difficulties - the medium is likely to be inhomogeneous with unknown properties, objects which scatter sound are usually present, and there are practical difficulties in positioning (and moving) the acoustic sensors. A suitable acoustic system might consist of a number of acoustic sensors positioned in the suspected locality of the sound source (Fig. 1).

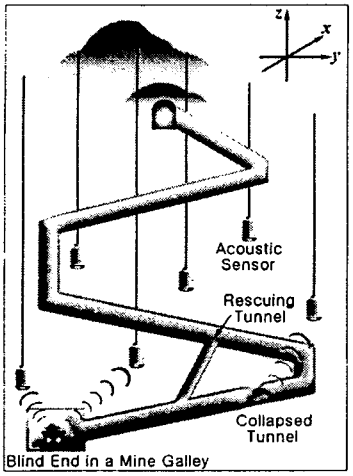


Fig. 1 An underground passive SONAR system could be commercially applicable for safety rescue following collapse of mining tunnels.

Two types of sensors are considered for underground acoustic application. One is a

geophone and the other is a hydrophone. Both sensors are usually made of piezoelectric materials and are fabricated for their own purpose of use. Geophones are non-waterproof velocity-sensitive transducers and therefore they are used at or slightly below the ground surface. In the other hand, hydrophones are waterproof and pressure-sensitive, so that they can be located inside a deep underground water-filled tunnel. Most of hydrophones are normally functioning at the depth of more than 300m water pressure[4]. Both sensors receive underground elastic wave signals as well as various types of noise in their operation. Particularly, geophones might be more sensitive to unwanted surface noise associated with ground surface activity. In order to have less the environmental noise, hydrophones are preferred when only the underground elastic wave signal is to be acquired

For underground acoustic application, hydrophones need to be used as transducers since most of underground holes become naturally filled with water after they are vertically digged. Most of underground for the present work are granitic just a few meter below the ground surface. Even though the standard value of the wave propagation velocity is about 6000m/sec in granite[5], there could be many possible variations in practice. Fig. 2 shows an overall layout of underground experimental apparatus. An array of hydrophones receive acoustic signals which are transmitted from a sound generating source and are propagated through rocks and soils. There may be expected geometric and materialistic attenuation in intensity and severe affection of environmental noise. Each of hydrophones would receive such noise-induced signals with relative time delay and power attenuation because of the geometric difference of the distance between the sound origin and the position of each sensor. These time delays and/or power attenuations are the only information for the localization of the sound origin position[6].

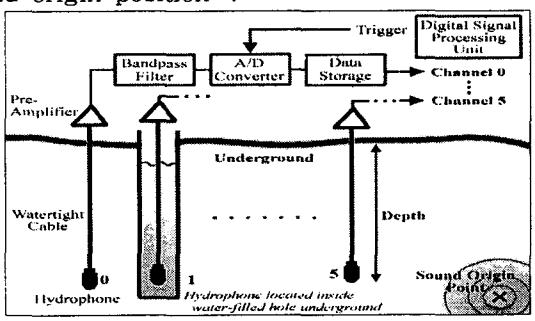


Fig. 2 The overall layout of the underground experimental apparatus

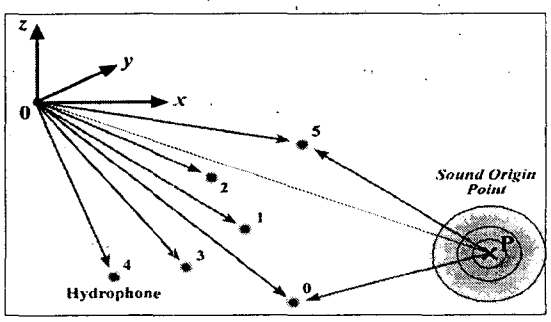


Fig. 3 The position of the underground sound origin could be evaluated from time delays and geographical coordinates.

The aim of this paper is to develope a complex underground acoustic system which detects and localizes the origin of an underground hammering sound using an array of hydrophones positioned about 100m underground. Three numerical estimating algorithms of the sound localization will be presented.

## 2. METHODS

6 underground holes were bored vertically to the ground. Their diameters are 15cm and the depth of each hole is about between 80m and 120m. After vertical drilling, the underground tunnels were naturally filled with water. A hydrophone was set at or near the bottom of each of the underground water-filled tunnels. Bruel & Kjaer type 8106 hydrophones were used (Table 1) with a 150m watertight low-impedance core cable (B&K AC0101) for the work.

Table 1. Characteristics of hydrophones [7]

| B & K Type no. | 8106 |
|---|---|
| Directivity | Omnidirection |
| Sensitivity (Voltage) | −174dB re 1V/$\mu$Pa |
| Electronic Components | Built−in 10 dB pre−amplifier with 7Hz high−pass filter |
| Frequency Range | +0.5 ~ −1.5 dB; 10Hz to 10KHz |
| Maximum Static Pressure | 260 dB/$\mu$Pa = $10^7$ Pa = 100 atm = 1000 m |
| Dimensions (L. x Dia.) mm | 182 x 32 |

The hydrophone receives underground elastic wave signals as well as various types of noise in their operation. The most disturbing noise is the 60Hz ground noise which is caused from the potential difference between the ground surface and the location of the hydrophone[8]. DC batteries were used in the complete acoustic system in order to remove such a 60Hz ground noise. Also the electrical line between the hydrophone and the system unit was completely shield[9]. Acoustic signals were amplified in 60dB constantly for all channels and were acquired with 10KHz sampling rate by a multi-channel A/D storage unit. DT-VEE package software was used as a data acquisition program[10]. In parallel with observation by a battery-operated digital storage oscilloscope, a headphone was used to perceive the environmental state inside the underground tunnel. Several locations inside an arbitrarily-made underground tunnel were prepared to be hammering origin positions on which a 10Kg hammer was stricken by a man.

Three different numerical methods were developed for underground acoustic sound localization. The first method is a time-delay method, the second method is a power-attenuation method and the third method is a hybrid method. The time-delay method uses relative time delay information between different input signals and the power-attenuation method uses relative power information between input signals. The hybrid method is a mixture of both methods. Since those methods carry out numerical solutions, more number of signal channels would improve estimating power in greater. In this work, six hydrophones were used.

## 2.1 TIME-DELAY METHOD

Consider six hydrophones randomly located underground (Fig. 3). Their global coordinates are $[x_i, y_i, z_i]$ for $(0 \le i \le 5)$. Any global position of the sound origin is assumed to be $[x_p, y_p, z_p]$. $\Delta T_{0i}$ is defined as a time delay between the first hydrophone and the $i^{th}$ hydrophone and V is the unknown velocity of the acoustic propagation. The first hydrophone is taken as a reference sensor while other hydrophones are considered as objective sensors. In the time-delay method, a sound origin is estimated by minimizing a cost function which relates distance differences between the $0^{th}$ sensor position and other sensor positions with time delays multiplied by the unknown sound propagation velocity;

$$F(x,y,z,V) = \sum_{i=1}^{5} ( r_i - r_0 - \Delta T_{0i} \cdot V )^2 \qquad (1)$$

where $r_0 = \sqrt{(x_0-x)^2+(y_0-y)^2+(z_0-z)^2}$ , $r_i = \sqrt{(x_i-x)^2+(y_i-y)^2+(z_i-z)^2}$ and [x, y, z] is an arbitrary coordinate. Different x, y, z, and V are applied to the cost function in order to find optimal values of x, y, z, and V which are an estimated sound origin and a propagation velocity.

Time delays between hydrophones are calculated by correlating one channel signal to the other[11];

$$\gamma_{xy}(m) = \frac{1}{N-|m|} \sum_{k=1}^{N-|m|-1} x(k)y^*(k+m) \qquad (2)$$

where N is the total number of discrete signals. It is an unbiased form of cross-correlation estimation. Since an input acoustic signal is mixed with various unwanted noise, the result of the correlation is often incorrect. It is always better to have higher sampling frequency in data acquisition.

## 2.2 POWER-ATTENUATION METHOD

A hammering shock generated from an underground tunnel is propagated to hydrophones through rocks and soils. From discrete pressure data, P(k), measured by the $i^{th}$ hydrophone, acoustic power, $I_i$, is calculated;

$$I_i = \frac{1}{N}\sum_{k=0}^{N-1} P^2_{S+N}(k) - \frac{1}{N}\sum_{k=0}^{N+1} P^2_N(k) \quad (3)$$

where subscripts S and N represent signal and noise. The attenuation of the acoustic power as underground elastic waves are propagated through underground media depends on distance and material properties. It might be modelled as follows[12];

$$I(r) = I_o \cdot (\frac{1}{r})^2 \cdot 10^{\alpha(r-1)} \quad (4)$$

where $\alpha$ is material attenuation coefficient [dB/M] and $I_o$ is an initial power of the hammering shock.

In the power-attenuation method, a sound origin is estimated by minimizing a cost function which relates measured power ratios between the $1^{st}$ sensor and other sensors with modelled power ratios;

$$F(x,y,z,\alpha) = \sum_{i=1}^{5}[\Delta P_{0i} - (\frac{r_i}{r_0})^2 \cdot 10^{\alpha(r_i - r_0)}]^2 \quad (5)$$

where $\Delta P_{0i}$ (= $I(r_0)/I(r_i)$) is defined as a power ratio between the first hydrophone and the $i^{th}$ hydrophone.

## 2.3 HYBRID METHOD

Both time-delay method and power-attenuation methods could be coupled together to derive a new cost function;

$$F(x,y,z,V,\alpha) = \sum_{i=1}^{5}\{K \cdot [\Delta P_{0i} - (\frac{r_i}{r_0})^2 \cdot 10^{\alpha(r_i - r_0)}]^2 + [r_i - r_0 - \Delta T_{0i} \cdot V]^2\} \quad (6)$$

where K is a weighting factor. In the hybrid method, both time-delay and power-attenuation information are used to estimate the sound source origin.

The algorithm of the Nelder-Meade simplex search method is used for estimating (x, y, z), $\alpha$ and V[13,14] from 6 measured acoustic powers. According to the simplex search algorithm, a simplex in n-dimensional space is characterized by the n+1 distinct vectors which are its vertices. In 5-space for the present case, a simplex is a hexagon. At each step of the search, a new point in or near the current simplex is generated. The function value at the new point is compared with the function values at the vertices of the simplex and, usually, one of the vertices is replaced by the new point, giving a new simplex. This step is repeated until the diameter of the simplex is less than the specified tolerance.

## 3. RESULTS AND DISCUSSION

Table 2 shows cartesian co-ordinates of 6 hydrophones located at the bottom of the water-filled tunnel. Z-axis is based on sea surface as 0m. There might be practically expected

some spatial deviation in sensor position because any vertical drilling underground could be twisted. The exact sensor position is not known. Fig.4 schematically shows 6 hydrophones' locations and a hammering position

Table 2. 6 hydrophone locations and a hammering position

| Sensor No. | X axis [m] | Y axis [m] | Z axis [m] | Distance from Hammering Position [m] |
|---|---|---|---|---|
| 0 | 593.5 | 671.4 | 338.7 | 99.8 |
| 1 | 608.7 | 656.4 | 366.8 | 98.4 |
| 2 | 688.3 | 600.2 | 376.3 | 122.1 |
| 3 | 673.6 | 594.2 | 354.9 | 124.0 |
| 4 | 701.0 | 644.8 | 341.7 | 74.9 |
| 5 | 668.1 | 640.3 | 371.7 | 84.3 |
| Hammering Position | 682.0 | 717.3 | 342.3 | 0 |

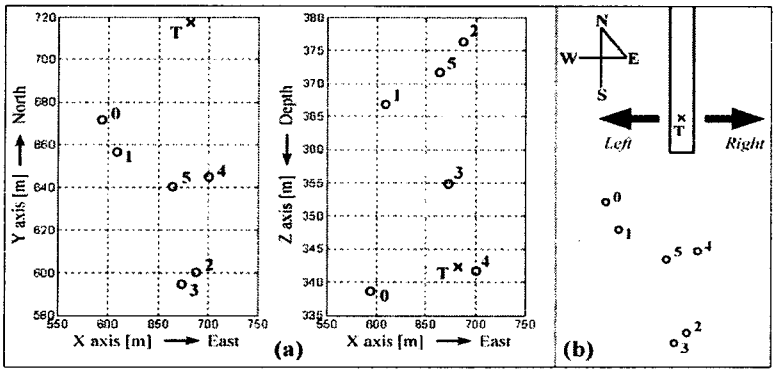


Fig. 4 hydrophone locations (o) and a hammering position (x)

Fig. 5 shows typical time responses of hammering stimuli on the underground tunnel. And Fig. 6 shows the FFT spectra of the corresponding time responses. It is meaningful to notice that even though the spectrum of each time response is calculated for the same hammering event, the pattern of the spectrum is significantly different from each other. This is interpreted as that the elastic wave of the hammering shock is changed in its spectrum while it is propagated through soils and rocks. Because of this phenomena, it is always difficult to calculate correct time delays between received signals by cross correlation technique[15].

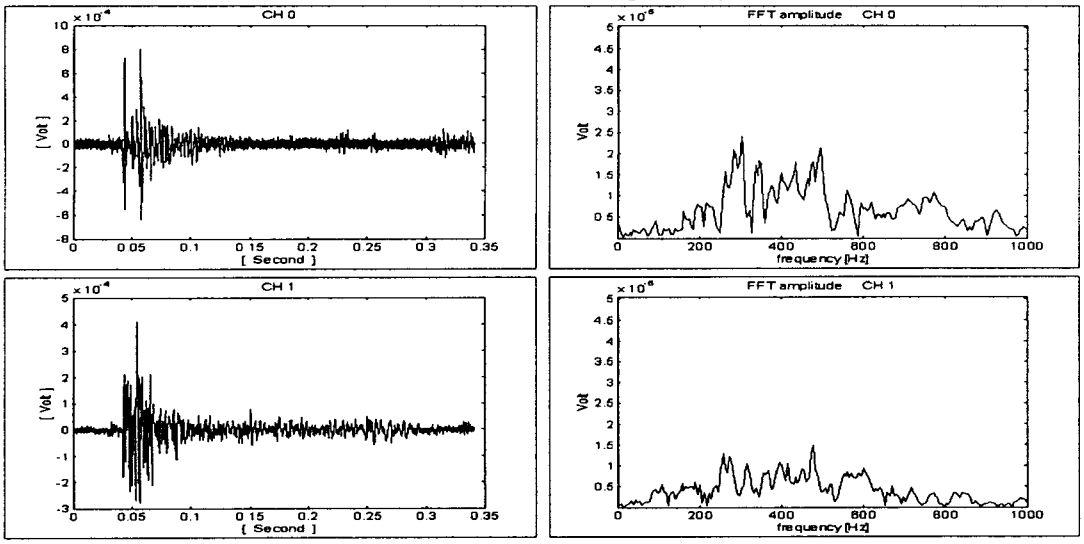

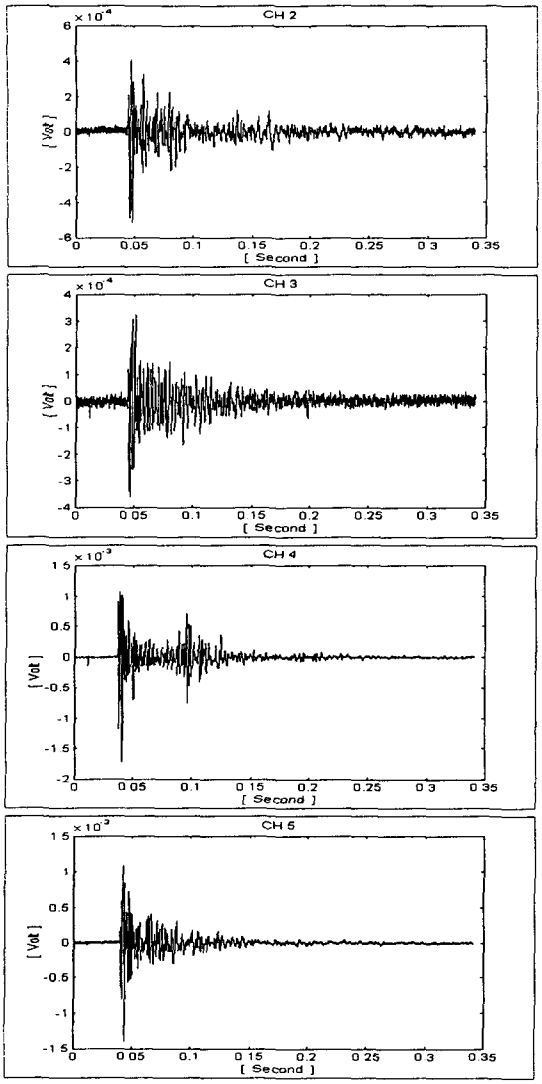


Fig. 5 Time Responses of Underground Hammering Shocks

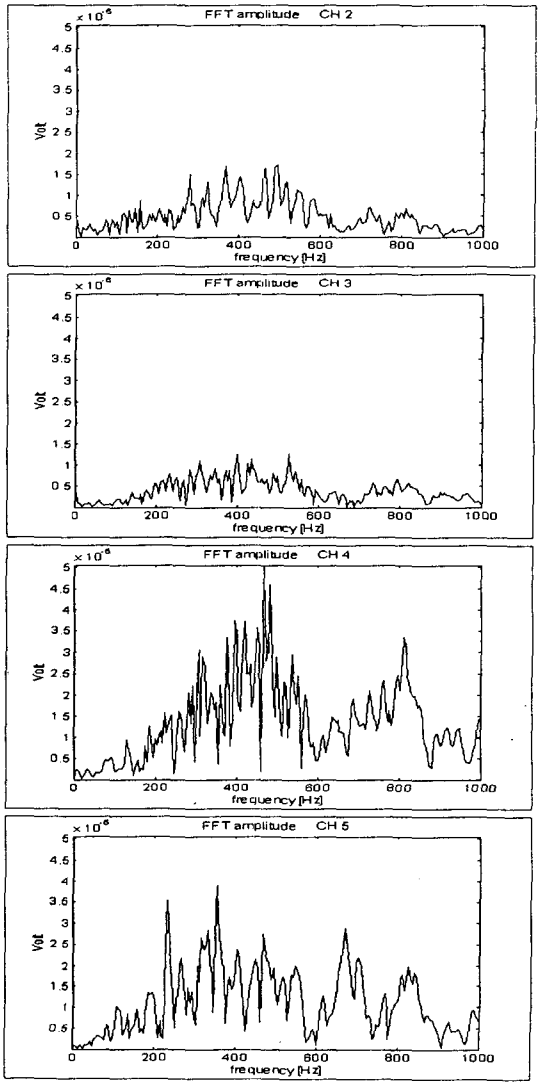


Fig. 6 FFT Spectra of Underground Hammering Shocks

### 3.1 TIME-DELAY METHOD RESULTS

A time delay can be theoretically calculated if the difference, between one distance which is between a reference sensor position and the sound origin and the other distance for the other objective sensor position, and the sound propagation velocity are known. Table 3 shows theoretical time delays between different reference sensors and objective sensors. The sound propagation velocity is assumed to be between 5000m/sec and 7000m/sec. Measured time delays are assumed to be in those range, but real data are occasionally quite different from theoretical values.

Table 4 shows measured time delays between different reference sensors and objective sensors. Time delay values are not diagonally symmetrical because of noise in the signal. There are quite significant differences between Table 3 and Table 4.

Table 3 Theoretical time delays between different reference sensors and objective sensors. (V=5000m/sec ~ 7000m/sec) [$10^{-3}$sec]

| Ref.\Obj. | 0 | 1 | 2 | 3 | 4 | 5 |
|---|---|---|---|---|---|---|
| 0 | 0.0 | −0.2~−0.3 | 3.2~4.5 | 3.5~4.9 | −3.5~−5.0 | −2.2~−3.1 |
| 1 | 0.2~0.3 | 0.0 | 3.4~4.7 | 3.7~5.1 | −3.3~−4.7 | −2.0~−2.8 |
| 2 | −3.2~−4.5 | −3.4~−4.7 | 0.0 | 0.3~0.4 | −6.7~−9.4 | −5.4~−7.6 |
| 3 | −3.5~−4.9 | −3.7~−5.1 | −0.3~−0.4 | 0.0 | −7.0~−9.8 | −5.7~−7.9 |
| 4 | 3.5~5.0 | 3.3~4.7 | 6.7~9.4 | 7.0~9.8 | 0.0 | 1.3~1.9 |
| 5 | 2.2~3.1 | 2.0~2.8 | 5.4~7.6 | 5.7~7.9 | −1.3~−1.9 | 0.0 |

Table 4 Measured time delays between different reference sensors and objective sensors. [$10^{-3}$sec]

| Ref.\Obj. | 0 | 1 | 2 | 3 | 4 | 5 |
|---|---|---|---|---|---|---|
| 0 | 0.0 | 0.2 | 4.3 | 4.4 | −3.4 | −1.2 |
| 1 | −0.3 | 0.0 | 4.0 | 4.1 | −4.2 | −1.4 |
| 2 | −4.3 | −4.0 | 0.0 | 0.2 | −8.1 | −5.3 |
| 3 | −4.4 | −4.1 | −0.1 | 0.0 | −8.3 | −5.5 |
| 4 | 3.4 | 4.3 | 8.0 | 8.2 | 0.0 | 2.8 |
| 5 | 1.2 | 1.4 | 5.2 | 5.5 | −2.8 | 0.0 |

Table 5 shows the estimated location of the sound origin and the estimated sound propagation velocity by the time-delay method. The estimated location with the 1st reference sensor is much closer to the true origin than those with the 6th reference sensor.

Table 5 The difference between the true origin and the estimated location by the time-delay method

| Reference Channel No. | Difference between the true origin and the estimated location [m] | | | | Estimated Velocity [m/sec] |
|---|---|---|---|---|---|
| | dX | dY | dZ | $\sqrt{dZ^2+dY^2+dZ^2}$ | |
| 0 | 1.996 | 10.000 | −10.050 | 14.3174 | 6500 |
| 1 | 5.996 | 18.000 | −13.050 | 23.0273 | 6330 |
| 2 | 12.000 | 29.000 | −16.050 | 35.2506 | 6439 |
| 3 | 7.996 | 19.000 | −17.050 | 26.7514 | 6390 |
| 4 | 6.996 | 20.000 | −22.050 | 30.5802 | 6359 |
| 5 | 21.000 | 44.000 | −18.050 | 51.9885 | 6637 |

One of comparative methods to find any reason of the difference between the true origin and the estimated location of Table 5 is normalizing distance differences (Table 6) as well as normalizing measured time delays (Table 7). In Table 6 distance differences between the distance between the reference sensor and the sound origin and the distances between objective sensors and the sound origin are normalized. And In Table 7 measured time delays are normalized with each of reference sensors. And Table 8 shows the difference between Table 6 and Table 7.

Table 6 Normalized distance differences with each of reference sensors

| Ref.\Obj. | 0 | 1 | 2 | 3 | 4 | 5 |
|---|---|---|---|---|---|---|
| 0 | 0.0000 | −0.0555 | 0.8994 | 0.9775 | −1.0000 | −0.6221 |
| 1 | 0.0537 | 0.0000 | 0.9244 | 1.0000 | −0.9143 | −0.5485 |
| 2 | −0.4753 | −0.5027 | 0.0000 | 0.0411 | −1.0000 | −0.8011 |
| 3 | −0.4943 | −0.5224 | −0.0395 | 0.0000 | −1.0000 | −0.8089 |
| 4 | 0.5057 | 0.4776 | 0.9605 | 1.0000 | 0.0000 | 0.1911 |
| 5 | 0.3889 | 0.3542 | 0.9512 | 1.0000 | −0.2362 | 0.0000 |

The absolute sum of each column indicates how much the corresponding sensor falsely

influences to other sensors in the calculation of the time delay. In Table 8 the 6th sensor has the highest value, 1.008, than other sensors. That is why the difference between the true origin and the estimated location with the 6th reference sensor is bigger than others in Table 5. Fig. 7 and Fig. 8 show differences between normalized theoretical distance differences (O) and normalized measured time delays (X) with the 1st reference sensor and the 6th reference sensor respectively.

Table 7 Normalized time delays with each of reference sensors

| Ref. \ Obj. | 0 | 1 | 2 | 3 | 4 | 5 |
|---|---|---|---|---|---|---|
| 0 | 0.0000 | 0.0455 | 0.9773 | 1.0000 | −0.7727 | −0.2727 |
| 1 | −0.0714 | 0.0000 | 0.9524 | 0.9762 | −1.0000 | −0.3333 |
| 2 | −0.5309 | −0.4938 | 0.0000 | 0.0247 | −1.0000 | −0.6543 |
| 3 | −0.5301 | −0.4940 | −0.0120 | 0.0000 | −1.0000 | −0.6627 |
| 4 | 0.4146 | 0.5244 | 0.9756 | 1.0000 | 0.0000 | 0.3415 |
| 5 | 0.2182 | 0.2545 | 0.9455 | 1.0000 | −0.5091 | 0.0000 |

Table 8 Differences between normalized distance differences and normalized time delays

| Ref. \ Obj. | 0 | 1 | 2 | 3 | 4 | 5 |
|---|---|---|---|---|---|---|
| 0 | 0.0000 | 0.1010 | 0.0779 | 0.0225 | 0.2273 | 0.3494 |
| 1 | −0.1251 | 0.0000 | 0.0280 | −0.0238 | −0.0857 | 0.2152 |
| 2 | −0.0556 | 0.0089 | 0.0000 | −0.0164 | 0.0000 | 0.1468 |
| 3 | −0.0358 | 0.0284 | 0.0275 | 0.0000 | 0.0000 | 0.1462 |
| 4 | −0.0911 | 0.0468 | 0.0151 | 0.0000 | 0.0000 | 0.1504 |
| 5 | −0.1707 | −0.0997 | −0.0057 | 0.0000 | −0.2729 | 0.0000 |
| $\sum \lvert x \rvert$ | 0.4783 | 0.2848 | 0.1542 | 0.0627 | 0.5859 | 1.0080 |

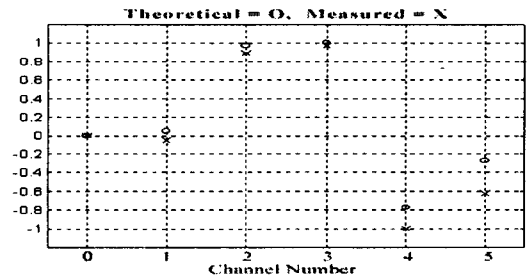


Fig. 7 Differences between normalized theoretical distance differences (O) and normalized measured time delays (X) with the 1st reference sensor

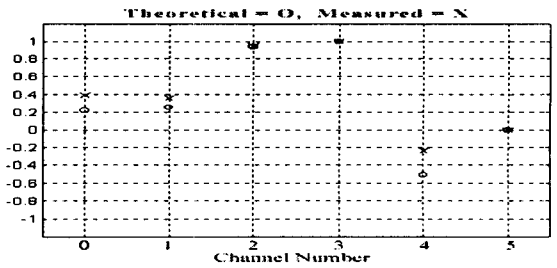


Fig. 8 Differences between normalized theoretical distance differences (O) and normalized measured time delays (X) with the 6th reference sensor

## 3.2 POWER-ATTENUATION METHOD RESULTS

Table 9 shows measured power ratios between different reference signal channels and objective signal channels. And Table 10 shows the estimated location of the sound origin and the estimated attenuation coefficient by the power-attenuation method. The estimated location with the 6th reference sensor is much closer to the true origin than those with the 2nd reference sensor. Fig. 9 shows the measured acoustic power (X) and numerically estimated power (O) of the hammering shock against distance. The continuous line indicates the trend of the acoustic power attenuation against distance with $\alpha$=0.0164 which is an optimized attenuation coefficient. The upper and the lower dashed lines are the bounds of the power attenuation. The attenuation coefficients for the upper and lower bounds are 0.0205 and 0.0131

respectively.

Table 9 Measured power ratios between different reference signal channels and objective signal channels

| Ref. \ Obj. | 0 | 1 | 2 | 3 | 4 | 5 |
|---|---|---|---|---|---|---|
| 0 | 1.0000 | 0.3745 | 0.5637 | 0.3320 | 4.1197 | 2.6409 |
| 1 | 2.6701 | 1.0000 | 1.5052 | 0.8866 | 11.0000 | 7.0515 |
| 2 | 1.7740 | 0.6644 | 1.0000 | 0.5890 | 7.3082 | 4.6849 |
| 3 | 3.0116 | 1.1279 | 1.6977 | 1.0000 | 12.4070 | 7.9535 |
| 4 | 0.2427 | 0.0909 | 0.1368 | 0.0806 | 1.0000 | 0.6410 |
| 5 | 0.3787 | 0.1418 | 0.2135 | 0.1257 | 1.5599 | 1.0000 |

Table 10 The difference between the true origin and the estimated location by the power-attenuation method

| Reference Channel No. | Difference between the true origin and the estimated location [m] | | | | Estimated Attenuation |
|---|---|---|---|---|---|
| | dX | dY | dZ | $\sqrt{dZ^2+dY^2+dZ^2}$ | |
| 0 | −9.891 | −20.56 | −7.631 | 24.0578 | 0.02120 |
| 1 | −19.00 | −64.00 | −15.050 | 68.4361 | 0.03192 |
| 2 | 9.996 | −14.00 | 12.950 | 21.5319 | 0.01404 |
| 3 | 0.996 | −18.00 | 5.952 | 18.9847 | 0.01736 |
| 4 | −11.00 | −41.00 | 7.048 | 43.0311 | 0.01712 |
| 5 | 8.532 | −5.901 | 14.40 | 17.7476 | 0.01801 |

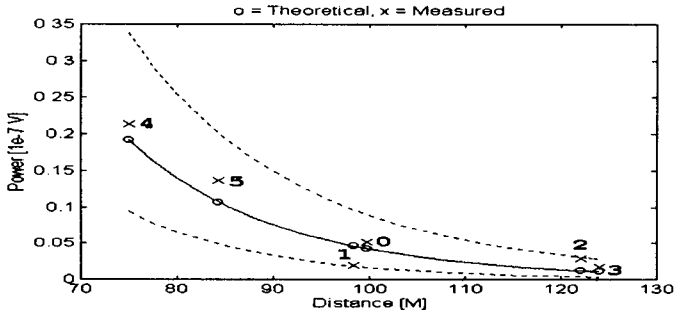


Fig. 9 Measured acoustic power (X) and numerically estimated power (O) of the hammering shock against distance. The continuous line indicates the trend of the acoustic power attenuation against distance.

The localization error of Table 10 is mainly caused by environmental noise in measurements. With the optimized attenuation coefficient, $\alpha$=0.0164, power ratios between different reference signal channels and objective signal channels can be theoretically calculated using Equ. (4) as in Table 11. And Table 12 shows differences between theoretical power ratios and measured power ratios for different reference sensors respectively. The most significant difference happens for the 2nd reference sensor such as 1295.5%.

Table 11 Theoretical power ratios with α=0.0164 between different reference signal channels and objective signal channels

| Ref. \ Obj. | 0 | 1 | 2 | 3 | 4 | 5 |
|---|---|---|---|---|---|---|
| 0 | 1.0000 | 1.0830 | 0.2878 | 0.2593 | 4.5161 | 2.5051 |
| 1 | 0.9234 | 1.0000 | 0.2658 | 0.2394 | 4.1700 | 2.3131 |
| 2 | 3.4741 | 3.7624 | 1.0000 | 0.9007 | 15.6893 | 8.7028 |
| 3 | 3.8571 | 4.1772 | 1.1102 | 1.0000 | 17.4189 | 9.6622 |
| 4 | 0.2214 | 0.2398 | 0.0637 | 0.0574 | 1.0000 | 0.5547 |
| 5 | 0.3992 | 0.4323 | 0.1149 | 0.1035 | 1.8028 | 1.0000 |

Table 12 Difference between theoretical power ratios and measured power ratios for different reference sensors respectively [%]

| Ref. \ Obj. | 0 | 1 | 2 | 3 | 4 | 5 | $\sum \lvert x \rvert$ |
|---|---|---|---|---|---|---|---|
| 0 | 0.0000 | 65.3979 | 96.3732 | 28.2906 | 8.7614 | 5.3891 | 204.2 |
| 1 | 188.9994 | 0.0000 | 467.5173 | 270.7592 | 163.6790 | 204.5738 | 1295.5 |
| 2 | 49.0766 | 82.3794 | 0.0000 | 34.6700 | 53.5382 | 46.3322 | 266.0 |
| 3 | 22.0520 | 73.0283 | 53.0690 | 0.0000 | 28.8813 | 17.8513 | 194.9 |
| 4 | 9.6027 | 62.0751 | 115.2304 | 40.6100 | 0.0000 | 15.5093 | 243.0 |
| 5 | 5.1135 | 67.1672 | 86.3316 | 21.7305 | 13.4269 | 0.0000 | 193.8 |

## 3.3 HYBRID METHOD RESULTS

Table 13 shows the estimated location of the sound origin, the estimated sound propagation velocity and the estimated attenuation coefficient by the hybrid method. The estimated location with the 2nd reference sensor is much closer to the true origin than those with the 5th reference sensor.

Table 13 The difference between the true origin and the estimated location by the hybrid method

| Reference Channel No. | Difference between the true origin and the estimated location [m] | | | | Estimated Velocity | Estimated Attenuation | Weight K |
|---|---|---|---|---|---|---|---|
| | dX | dY | dZ | $\sqrt{dZ^2+dY^2+dZ^2}$ | | | |
| 0 | −1.004 | 4.001 | −9.048 | 9.938 | 6460 | 0.02456 | 20 |
| 1 | −1.954 | 0.02904 | −4.728 | 5.116 | 6388 | 0.04120 | 7 |
| 2 | 5.996 | 0.001 | −4.048 | 7.235 | 6139 | 0.01303 | 125 |
| 3 | 3.113 | 2.872 | −3.181 | 5.297 | 6334 | 0.01750 | 23 |
| 4 | 10.30 | 24.50 | −16.87 | 31.4792 | 6451 | 0.01751 | 600 |
| 5 | −3.958 | −4.835 | −2.112 | 6.5957 | 6762 | 0.02064 | 1300 |

## 4. CONCLUSION

Both the time-delay method and the power-attenuation method produce just reasonable results of underground sound localization. The results of Table 13 by the hybrid method could be accepted to be applicable to practical application. If the 10Kg hammering shock is usually happening events inside an unknown covert tunnel, the present hydrophone with its own sensitivity could receive such underground acoustic pressures in the range of 250m radius. After several detections and localizations for the similar hammering events, the statistically averaged estimated origin of the hammering shock might be closer to the true origin. With such estimation of less than 30m difference, the true origin of the hammering location could

be discovered by a geophone at the suspected area[2,3].

In the present underground localization, the sound propagation velocity and the power attenuation coefficient of the underground media are assumed to be constant for every channels for simplicity. The propagation velocity and the attenuation coefficient could be variable in the real underground media. And there would be diverse elastic wave propagation phenomena; reflection, reverberation, abruption, scattering etc.. The difference between the true position of the arbitrarily-made sound source and the numerically estimated position is caused by such a complex phenomena under the ground. The present underground acoustical system need to be practically used in parallel with statistical averaging techniques to find out the position of an unknown underground excavation/hammering event. If there is expected to have a critical parameter such as abrupt media variation, each of channels is to be calibrated in order to account the variation of the propagation velocity and/or the attenuation coefficient.

ACKNOWLEDGMENTS

This study was carried out with the computing facilities (Cray T3E) of the super computer centre at SERI (now at ETRI) in Korea, and was granted by STEPI (Science & Technology Policy Institute) Korea, as 1998 international program of co-work of research between Korea and United Kingdom.

## 5. REFERENCES

[1] Ballard R.F., "Tunnel Detection" U.S. Army Engineer Waterways Experiment Station, Technical Report GL-82-9, 1982.
[2] Greenfield R.J., "Seismic Analysis of Tunnel Boring Machines Signals at Kerckhoff Tunnel", U.S. Army Engineer Waterways Experiment Station, Miscellaneous Paper GL-83-19, 1983.
[3] Greenfield R.J., "The WES Seismic Listening System (SLS)", reported by U.S. Army Engineer Waterways Experiment Station, Vicksburg, Mississippi, 1987.
[4] Stansfield D., "Underwater Electroacoustic Transducers", Bath University Press and Institute of Acoustics 1990.
[5] ASNT (American Society of Non-destructive Testing) Handbook, 2nd Edition, Vol. 5 Acoustic Emission Testing, pp:314, 1991.
[6] Coates R.F.W., "Underwater Acoustic Systems", Macmillan Education Ltd., 1990.
[7] *Brüel & Kjaer*, "Sound & Vibration Product Catalogue", printed by B & K, 1995.
[8] Horowitz P. and Hill W. "The Art of Electronics", Cambridge University Press, Cambridge, pp:457-466, 1990.
[9] Jarng S.S., Park J.A., Rhee K.H., "Development of underground acoustic noise rejection method", Basic Science and Eng., The Int. J. of Chosun Uni., vol.1 no. 2, pp:1035-1041, 1997.
[10] Data Acquisition with DT VEE, printed by Data Translation U.S.A., 1995.
[11] J.S. Bendat and A.G. Piersol, "Random Data: Analysis and Measurement Procedures", p. 332, John Wiley and Sons, 1971.
[12] Ben-menahem A. and Singh S.J. "Seismic Waves and Sources", published by Springer-Verlag, pp. 1056, 1981.
[13] Nelder J.A. and Mead R., "A simplex method for function minimization", Computer Journal, Vol. 7, PP:308-313. 1965.
[14] Dennis J.E., Jr. and Woods D.J., "New computing environments microcomputers in large-scale computing", edited by A.Wouk, SIAM, PP:116-122, 1987.
[15] A.V. Oppenheim and R.W. Schafer, "Digital Signal Processing", Prentice-Hall, pp.539, 1975.